ARTICLE

First Member of an Appealing Class of Cyclometalated 1,3-Di-(2-Pyridyl)Benzene Platinum(II) Complexes for Solution-Processable OLEDs

Received 00th January 20xx,
Accepted 00th January 20xx

DOI: 10.1039/x0xx00000x

Claudia Dragonetti[a], Francesco Fagnani[a], Daniele Marinotto[b], Armando di Biase[a], Dominique Roberto[a], Massimo Cocchi,[c,]* Simona Fantacci[d,]* and Alessia Colombo[a,]*

The preparation and characterization of a new platinum(II) complex bearing a N^C^N-cyclometalating ligand and a thiolate coligand, namely 5-mesityl-1,3-di-(2-pyridyl)benzene and 1-phenyl-1H-tetrazole-5-thiolate, is reported. Its structure is determined by X-ray diffraction studies on a single crystal. This new complex exhibits green and red phosphorescence in dichloromethane solution (Φ_{lum} = 0.90) and in the solid state (Φ_{lum} = 0.62), respectively. In both cases the quantum yield is impressive showing for the first time that N^C^N platinum(II) complexes with a suitable thiolate can reach outstanding luminescent properties. The excellent solubility of this complex allows to fabricate green processable solution-OLEDs with maximum EQE similar to that obtained with more expensive vacuum techniques and, depending on its concentration, one can tune the color of the OLED. The molecular geometry, ground state, electronic structure, and excited electronic states of the complex, both as monomer and dimer aggregate in solution, are calculated by density functional theory (DFT) and time-dependent DFT approaches, giving insight into the electronic origin of the absorption spectra. Remarkably, the dimer is less sensitive to oxygen quenching than the monomer because the two 1-phenyl-1H-tetrazole fragments protect the platinum(II) centers, as suggested by a combination of luminescence studies and theoretical calculations.

1. Introduction

Metal complexes attract enormous interest for organic light-emitting diodes (OLEDs) because of the great emission efficiencies that they may give[1-4] thanks to the intersystem crossing caused by the metal which allows emission from the otherwise lost triplet states that are up to three-quarters of the excited states obtained upon charge-recombination in electroluminescent devices.[5,6] Meanwhile, such metal complexes are also of interest for sensing and bio-imaging.[7-13] Particularly appealing for optoelectronics are square planar platinum(II) complexes, because of the parallel emissions from bi-molecular and mono-molecular excited states which allow tuning of the efficiency and color of OLEDs.[14-17] The square planar geometry of the Pt complexes enables the formation of bi-molecular states, either in the excited states (excimers) or in the ground states (dimers), thanks to intermolecular interactions of Pt-Pt or ligand-ligand or both.[18] In particular, platinum(II) chloride complexes with a terdentate ligand based on cyclometalated 1,3-di(2-pyridyl)benzene (dpyb), which gives platinum an N^C^N coordination environment, are fascinating.[19-23] These compounds are the brightest platinum emitters in solution at room temperature. Thus, [Pt(dpyb)Cl] has a luminescence quantum yield (Φ_{lum}) of 0.60 in deaerated CH_2Cl_2,[19] one order of magnitude higher than that of the related [Pt(N^C-ppy)(N-ppyH)Cl] (ppyH is 2-phenylpyridine) complex[24] or its N^N^C isomer,[25] although the single ligating units are the same.[22] This remarkable luminescence is explained by the superior rigidity of the N^C^N ligand, which inhibits the distortion that causes non-radiative decay in the bidentate moiety, and the short Pt–C bond which leads to a particularly high ligand-field strength.[19-23] The charm of these bright platinum(II) complexes, which found successful applications in OLEDs[26-34] and bio-imaging,[35-37] is enhanced by the capacity to modulate the emission color through introduction of substituents on the pyridyl or phenyl rings, keeping high the quantum yields.[17] Surprisingly, whereas much work has been devoted to better understand the effect of the substituents on the N^C^N ligand, the study of the influence of the coligand on the emission properties is still in its infancy. Substitution of the chloride with an acetylide[31] or isothiocyanate[32] leads to highly luminescent complexes in solution (Φ_{lum} = 0.60-0.77) whereas Pt-OPh complexes have half the value of the quantum yields of the related Pt-Cl complexes indicating that the coligands have an influence on

[a.] *Dipartimento di Chimica, Università degli Studi di Milano, UdR INSTM di Milano, via C. Golgi 19, 20133 Milano, Italy*
[b.] *Istituto di Scienze e Tecnologie Chimiche (SCITEC) "Giulio Natta", Consiglio Nazionale delle Ricerche (CNR), via C. Golgi 19, 20133 Milan, Italy*
[c.] *Istituto per la Sintesi Organica e la Fotoreattività (ISOF), Consiglio Nazionale delle Ricerche (CNR), via P. Gobetti 101, 40129 Bologna, Italy*
[d.] *Computational Laboratory for Hybrid/Organic Photovoltaics (CLHYO), CNR-SCITEC, via Elce di Sotto 8, I-06213, Perugia, Italy*

†Electronic Supplementary Information (ESI) available: NMR-spectra and photoluminescence properties in solution and in the solid state.
See DOI: 10.1039/x0xx00000x

the excited state properties of [Pt(dpyb)X] complexes, although the excited state is localized mainly in the Pt(N^C^N) moiety.[38] Although their luminescence quantum yield is lower, [Pt(dpyb)(OPh)] complexes provide an avenue to design chloride-free phosphorescent emitters, useful to increase the operational stability of OLEDs.[26,38] Besides, it was reported that arenethiolate (-SPhR) coligands lead to red luminescence in solution due to charge-transfer transition from the platinum/thiolate to the N^C^N ligand, but the quantum yields are low (Φ_{lum} = 0.17, 0.069, 0.014 and 0.002 for R=H, CH_3, OCH_3, NO_2, respectively).[39]

This contribution shows the fascinating and unexpected effect of changing the coligand in such complexes from chloride to 1-phenyl-1H-tetrazole-5-thiolate (Figure 1). Contrarily to the known [Pt(dpyb)SPhR], in solution this novel complex is highly luminescent in the green region and has, to our knowledge, the highest quantum yield reported for a (N^C^N)platinum(II) emitter. This fascinating complex is highly emissive also in the solid state, in the red region, and has an excellent solubility affording a springboard for the preparation of efficient and convenient solution-processable OLEDs. It opens a new horizon for the design and use of cyclometallated 1,3-di-(2-pyridyl)benzene platinum(II) complexes.

2. EXPERIMENTAL

2.1 Synthesis of [Pt(5-mesityl-dpyb)(SCN_4Ph)]

Complex [Pt(5-mesityl-dpyb)Cl] (prepared as previously reported,[33] 110 mg, 0.189 mmol) was dissolved in acetone (250 mL) under argon and 1-phenyl-1H-tetrazole-5-thiol sodium salt (515 mg, 2.572 mmol) was added to the solution. The obtained mixture was stirred at room temperature in the darkness for 24 hours. The precipitation of an orange solid was observed. The desired product, [Pt(5-mesityl-dpyb)(SCN_4Ph)], was recovered by filtration (129 mg, 0.02 mmol, 94%).

^{1}H NMR (400 MHz, CD_2Cl_2, δ): 9.20 (d, J = 4.9 Hz, 2H), 7.99 (td, J_1 = 7.7 Hz, J_2 = 1.2 Hz, 2H), 7.88 (d, J = 7.6 Hz, 2H), 7.71 (d, J = 7.7 Hz, 2H), 7.50-7.40 (m, 3H), 7.34 (s, 2H), 7.26 (td, J_1 = 6.0 Hz, J_2 = 1.1 Hz, 2H), 7.02 (s, 2H), 2.38 (s, 3H), 2.13 (s, 6H).

^{13}C NMR (100 MHz, CD_2Cl_2, δ): 153.57, 151.36, 143.82, 139.85, 138.61, 136.38, 132.11, 129.23, 128.48, 125.54, 124.05, 120.00, 118.66, 30.08, 21.00.

Anal. calcd. for $C_{32}H_{26}N_6PtS.0.5CH_2Cl_2$: C 51.08, H 3.56, N 11.00; found: C, 51.58; H, 3.57; N,11.06.

2.2 Photophysical characterization

Electronic absorption spectra were obtained at room temperature in dichloromethane, by means of a Shimadzu UV3600 spectrophotometer and quartz cuvettes with 1 cm optical path length. Absolute photoluminescence quantum yields, Φ, were measured using a C11347 Quantaurus Hamamatsu Photonics K.K spectrometer, equipped with a 150 W Xenon lamp, an integrating sphere and a multichannel detector. Steady state and time-resolved fluorescence data were recorded with a FLS980 spectrofluorimeter (Edinburg Instrument Ltd). See details in ESI.

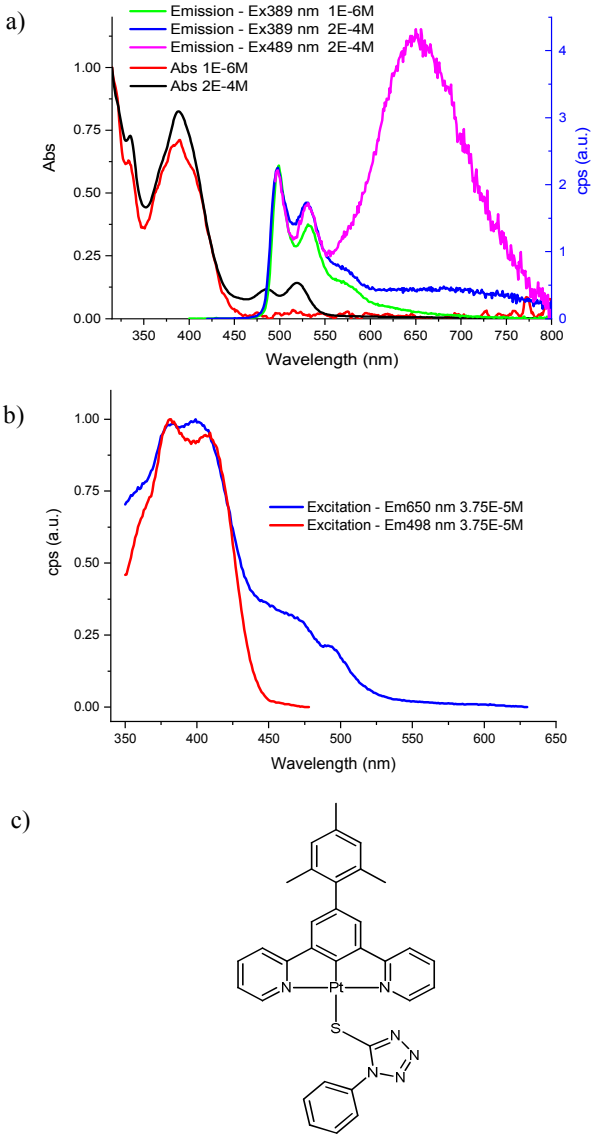

Figure 1. a) Normalised absorption spectra at concentrations of 1 x 10^{-6} M and 2 x 10^{-4} M and normalised emission spectra at 1 x 10^{-6} M and 2 x 10^{-4} M exciting at 389 and 489 nm in CH_2Cl_2 at 298 K; b) Excitation spectra recorded at 498 and 650 nm of the CH_2Cl_2 3.75 x 10^{-5} M solution; c) Molecular structure of complex [Pt(5-mesityl-dpyb)(SCN_4Ph)].

2.3 Computational Details

All the calculations were performed with Gaussian09 (G09)[40] without any symmetry constraints. The molecular geometry of [Pt(5-mesityl-dpyb)(SCN_4Ph)] and its dimer has been optimized by a Density Functional theory (DFT) approach using the B3LYP[41] exchange–correlation functional integrated with the D3-BJ model to contain the dispersion interactions,[42] which are mandatory to correctly optimize the dimer geometry. The 6-31G** basis set[43-45] has been employed for all atoms except

for Pt which has been described with LANL2DZ basis set[46] along with the corresponding pseudopotentials. We optimized the geometries in CH_2Cl_2 including solvation effects by means of the conductor-like polarizable continuum model (C-PCM)[47,48] as implemented in G09. Time Dependent DFT (TDDFT) calculations have been performed in CH_2Cl_2 solution for both [Pt(5-mesityl-dpyb)(SCN_4Ph)] and its dimer. The non-equilibrium version of the C-PCM was used for TDDFT calculations, as implemented in G09[49,50] To simulate the optical spectra, eighty (two hundred) singlet–singlet transitions have been computed for the monomer (dimer) and interpolated by Gaussian functions with σ = 0.12 eV.

2.4 X-ray structure determination

Crystal data. $C_{32}H_{26}N_6SPt \cdot 1/2CH_2Cl_2$, M = 764.20 g/mol, monoclinic, a = 20.869(2), b = 9.272(1), c = 29.834(3) Å, β = 92.711(2), V = 5766(2) $Å^3$, T = 200(2) K, space group $P2_1/n$ (No. 14), Z = 8, μ = (Mo−Kα) 5.066 mm^{-1}; 39824 reflections (10463 unique; Rint = 0.0882) were collected in the range 2.32° <2 θ < 50.58°, employing a 0.15 × 0.06 × 0.01 mm^3 crystal mounted on a BrukerAPEX II CCD diffractometer and using graphite-monochromatized Mo−Kα radiation (λ = 0.71073 Å). Data sets were corrected for Lorentz polarization effects and for absorption (Tmin = 0.699) (SADABS)[51]. The structure was solved by direct methods (SIR-92)[52] and was finished by iterative cycles of full-matrix least-squares refinement on Fo^2 and ΔF synthesis using the SHELXL-97[53] program (WinGX suite)[54]. Hydrogen atoms, were located on the ΔF maps and allowed to ride on their carbon atoms. Final R1 [wR2] values are 0.0618 [0.1264] on I > 2σ(I) [all data].

Crystallographic data for [Pt(5-mesityl-dpyb)(SCN_4Ph)], have been deposited with the Cambridge Crystallographic Data Centre as supplementary publication no. CCDC 1979249. These data can be obtained free of charge via www.ccdc.cam.ac.uk/conts/retrieving.html (or from CCDC, 12 Union Road, Cambridge CB2 1EZ, UK; fax: +44 1223 336033; e-mail: deposit@ccdc.cam.ac.uk).

2.5 Procedure for OLED fabrication and assessment

OLEDs were built by growing thin layers on clean glass substrates pre-coated with a 120 nm-thick layer of indium tin oxide (ITO) with a sheet resistance of 20 Ω per square. A 40 nm thick hole injecting layer of poly(3,4-ethylenedioxythiophene) polystyrene sulfonate (PEDOT:PSS, Clevios P VP AI 4083) was spin-coated (4000 rpm) and then the substrates were heated at 140 °C for 10 min. After the ITO/PEDOT:PSS substrates were cooled down, a 40 nm-thick film of the luminescent layer containing 8 wt% or 25 wt% of [Pt(5-mesityl-dpyb)(SCN_4Ph)] and 92 wt% or 75 wt% of 4,4',4''-tris(N-carbazolyl-triphenylamine (TCTA) was spin-coated (2000 rpm) from a 10 mg/mL CH_2Cl_2 solution in clean room environment. Electron transporting of 30 nm-thick 2,2',2"-(1,3,5-benzinetriyl)-tris(1-phenyl-1-H-benzimidazole) TPBi and cathode electrode of 0.5 nm-thick LiF with cap of 100 nm-thick Al were deposited in sequence by thermal evaporation under vacuum (10^{-6} hPa). The current-voltage features were obtained with a Keithley Source-Measure unit (model 236) under continuous operation mode, while the light output power was obtained with an EG&G power meter and electroluminescence spectra by a StellarNet spectroradiometer. All measurements were done under argon atmosphere at room temperature and were reproduced many times, excluding any irreversible chemical and morphological changes in the devices.

3. Results and discussion

3.1 Synthesis

The new complex [Pt(5-mesityl-1,3-di-(2-pyridyl)benzene)(1-phenyl-1H-tetrazole-5-thiolate)], [Pt(5-mesityl-dpyb) (SCN_4Ph)] , was readily prepared upon treatment of the related chloride complex with 1-phenyl-1H-tetrazole-5-thiol sodium salt in acetone at room temperature as reported above (see also Electronic Supplementary Information). It was fully characterized by NMR spectroscopy and elemental analysis.

3.2 Photophysical properties in solution

The absorption and photoluminescence spectra of [Pt(5-mesityl-dpyb)(SCN_4Ph)] in dichloromethane solution at dilute and elevated concentrations are shown in Figure 1.

The absorption spectrum in solution at dilute concentration ($1x10^{-6}$ M) shows the characteristic profile of intense absorption bands at 260–320 nm attributed to intraligand $^1\pi$-π* transitions of the N^C^N ligand and less intense bands at 350–460 nm assigned to charge-transfer transitions involving the cyclometalated ligand and the metal.[33] When the concentration increases, new absorption bands appear at lower energy with maxima at ca. 489 and 519 nm, due to aggregation of the platinum(II) complex as confirmed by a deviation from the Lambert-Beer law (see Electronic Supplementary Information, Figures S1-S3). This behavior is different from that of the related complexes [Pt(5-mesityl-dpyb)Cl] and [Pt(5-mesityl-dpyb)(NCS)] which follow the Beer-Lambert law, up to 10^{-4} M, ruling out the manifestation of significant aggregation with chloride and isothiocyanate as coligands.[33]

Upon excitation at 389 nm, [Pt(5-mesityl-dpyb)(SCN_4Ph)] is intensely phosphorescent, in the green region, in dilute dichloromethane solution at room temperature, showing a vibrationally structured emission spectrum with maxima at 498, 531 and 579 nm (Figure 1a), like the parent chloride and isothiocyanate derivatives,[33] that can be attributed to the monomeric complex. When the concentration of the monomer is increased up to 2×10^{-4} M, a structureless band around 650 nm is detected. This new band at lower energy, which increases drastically by varying the excitation wavelength from 389 to 489 nm (Figure 1a; Figure S5-S7), can be attributed to the emission from aggregate complexes such as dimers. In fact, the excitation spectra of a 3.8×10^{-5} M solution at the maximum of the emission spectrum of the monomer (498 nm) and at 650 nm are different (Figure 1b), confirming the assignment to a ground-state dimer rather than to an excimer.

Clearly an increase of the concentration leads to aggregation of [Pt(5-mesityl-dpyb)(SCN_4Ph)] to give dimeric species,[18] in contrast to the comportment of the chloride and isothiocyanate derivatives.[33]

Unexpectedly, in dilute deaerated dichloromethane solution ($1x10^{-6}$ M), the novel thiolate platinum (II) complex has an impressive luminescence quantum yield (Φ_{lum} = 0.90), considerably superior to that reported for the parent complexes (Φ_{lum} = 0.62 and 0.60, for X= Cl and NCS, respectively)[33] and much higher than that reported for other thiolate platinum(II) complexes (Φ_{lum} = 0.002-0.17).[39] The room temperature solution emission is very efficiently quenched by oxygen: it is 18 times lower in air-equilibrated dichloromethane (Table S1); given the efficacy of oxygen quenching, efficient production of singlet oxygen -the $^1\Delta g$ state of O_2 - can be anticipated. Increasing the complex concentration in deaerated dichloromethane solution caused a quenching of the luminescence quantum yield (Table S1 and Figure S4); a degassed 2 x 10^{-4} M solution showed the quantum yield to drop by a factor 7.5, reaching a value of 0.12. Interestingly, in air-equilibrated solution, the quantum yield of the 2 x 10^{-4} M solution decreases by a factor 4 only compared to the value recorded for the 1 x 10^{-6} M solution, suggesting that the aggregate complex is comparably less sensitive to oxygen quenching.

Excited state decay measurements of [Pt(5-mesityl-dpyb)(SCN_4Ph)] solutions at different concentrations were performed exciting at 374 nm at the emission wavelength of 498 nm (Electronic Supplementary Information, Table S1 and Figures S8-S12). At low concentration, a mono-exponential transient decay is observed for the monomer complex, with a lifetime of 7.39 μs, similar to that obtained for the chloride parent.[33] The radiative (K_r) and overall non-radiative (K_{nr}) rate constants are 1.23 x 10^5 s^{-1} and 1.38 x 10^4 s^{-1}, respectively.[18] An increase of the concentration leads to a bi-exponential transient decay (1 x 10^{-5} M, τ_1 = 0.79 μs (8.97%) τ_2 = 6.94 μs (91.03%); 2 x 10^{-4} M, τ_1 = 0.73 μs (72.11%) τ_2 = 2.43 μs (27.89%); Table S1) where the two lifetimes can be related to the presence of two different species in solution, most likely a monomeric and dimeric complex forms, by analogy with a related complex.[18] The formation of the dimer causes a diminution of the lifetime and quantum yield.

3.3 Computational modelling of monomer and dimer aggregates

To better understand the electronic transitions underlying the peculiar photophysical properties of the [Pt(5-mesityl-dpyb)(SCN_4Ph)] complex, with particular relation to aggregation, we carried out DFT and TDDFT calculations on the monomer and dimer complex starting from their structural optimization in dichloromethane solution, see left panel in Figure 2. The optimized structure of the monomeric platinum(II) complex is in good agreement with the X-ray structure (see below, "X-ray structure determination"), apart from the different orientation of the tetrazolic phenyl moiety. Notably, the dimer optimized geometry is also consistent with the X-ray determined solid state structure, showing a comparable orientation of the monomers, with a calculated Pt···Pt distance of 3.4 Å to be compared to the experimental values of ~3.37 Å, see below. As a check of our calculated structures we also optimized the monomer and the dimer with the tetrazolic phenyl in the same orientation as in the crystallographic structure, finding them to be less stable than the more stable solution-optimized structures by ~4 kcal/mol, suggesting that the precise orientation of the phenyl ring is likely affected by crystal packing forces. Remarkably, in the dimer aggregate, the two 1-phenyl-1H-tetrazole fragments give some protection to the platinum(II) centers. This shield reasonably explains why the aggregate complex is less sensitive to oxygen quenching than the monomer.

We have analyzed the electronic structure of the monomer complex and of its dimer, simulated their Uv-vis spectra, and characterized the excited states involved in the main absorption bands, see Figure 2. The simulated absorption spectra of the monomer (red line) and the dimer (blue line) are reported in the spectral range 300-600 nm, to focus on the charge-transfer character absorption bands.

The simulated monomer spectrum is representative of the experimental one measured in dilute solution ($1x10^{-6}$ M) whereas that of the dimer may be compared to the experimental spectrum at higher concentrations ($2x10^{-4}$ M).

The simulated monomer spectrum shows two low energy bands, one originated by the low intensity HOMO→LUMO transition at 421 nm, and one centered at the more intense HOMO-LUMO+1 transition at 410 nm. The electron density difference between the S_1 and S_2 excited states and the ground state (S_0) are reported in Figure 2 (red inset) to visualize the rearrangement of the electron density in the excited states. Both transitions show a directional charge-transfer $d_{Pt}/\pi_S \rightarrow \pi^*_{dyp}$ character, to be assigned as mixed metal/ligand to ligand' charge transfer (MLL'CT) transitions.

The simulated spectrum of the dimer shows an intensity increase and a red shift with respect to that of the monomer, in line with the behavior of the experimental spectrum at a higher concentration. The lowest absorption band at 503 nm is originated by the S_1 HOMO-LUMO transition, with the HOMO localized on both the metal centers, and the LUMO being a π* orbital delocalized on both dpyb ligands. The S1 electron density difference plot, blue inset in Figure 2, visualizes the electron density rearrangement upon excitation from the metal (electron density decrease, blue) to the dpby ligand (electron density increase, red) of both the monomer units ($d_{Pt} \rightarrow \pi^*_{dyp}$); S_1 is assigned as a ML'CT transition. The computed absorption band at 415 nm is generated by two essentially coincident transitions with the same intensity (S_7 and S_8), each one involving mainly one dimer unit. The analysis of the TDDFT eigenvectors and the isodensity plots of the S_7/S_8 electron density difference, (blue inset of Figure 2), show that both the excited states have a MLL'CT character and correlate with the transition at 420 nm of the monomer spectrum. The band at 503 nm is a peculiar feature of the dimer aggregate; this transition originates from the Pt center with no contribution of sulphur.

ARTICLE

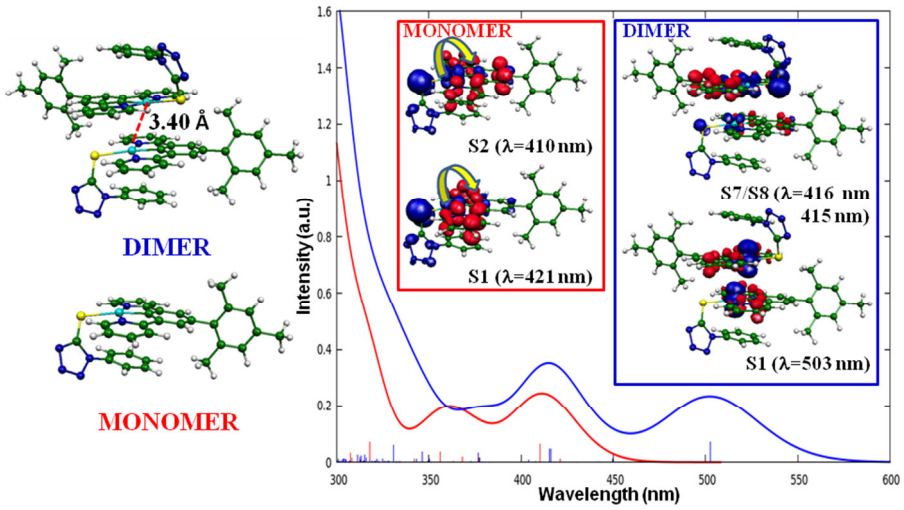

Figure 2. Left panel: Optimized geometry of [Pt(5-mesityl-dpyb)(SCN_4Ph)] monomer (bottom) and dimer (top). Right panel: Simulated absorption spectra of the monomer (red) and the dimer (blue). Red inset: Electron density difference plots of S1 and S2 monomer excited states. Blue inset: Electron density difference plots of S1 and S7/S8 dimer excited states. Blue and red colors indicate a decrease and increase, respectively, of the electron density upon excitation.

3.4 Photophysical properties in the solid state

For a lot of uses, like lighting devices or sensing, conserving luminescence in the solid state is a sought-after property.[55,56] However, compounds with highly emissive phosphorescence in dilute solutions often have the problem of "aggregation-caused quenching" in concentrated solutions or in the solid state; for example, [Ir(phenylpyridine)$_3$] is highly luminescent in dilute solution (0.97) but poorly luminescent in the solid state (0.004) because of self-quenching due to intermolecular $\pi-\pi$ stacking interactions.[56] A strategy to inhibit intermolecular interactions in the solid state is the introduction of bulky substituents.[57,58] We were curious to see the luminescent behavior of our novel complex in the solid state.

Remarkably, as powder at room temperature, [Pt(5-mesityl-dpyb)(SCN_4Ph)] is characterized by an impressive phosphorescence quantum yield of 0.62 at 703 nm (Figure S15), standing among the best quantum yields reported for Pt complexes in bulk solid (0.85 at 500 nm,[59] 0.51 at 522 nm,[56] 0.58 at 530 nm,[58] 0.52 at 640 nm,[55]). Interestingly, we found that the related complex with isothiocyanate as coligand doesn't emit as powder. The red-shift of the emission observed for [Pt(5-mesityl-dpyb)(SCN_4Ph)] on going from the concentrated solution (650 nm) to the solid state (703 nm) can be attributed to further aggregation of the Pt dimers. Exciting the powder at 374 nm at the emission wavelength of 703 nm, a mono-exponential decay is observed with a lifetime of 1.24 μs (Figure S16). At low temperature (77K), the emission band is slightly red shifted (maximum at 713 nm, Figure S17) and narrower due to the lower exciton diffusion toward trap sites (self-trapped state like dimers, trimers, excimer, etc.) in solid medium (powder) because generally exciton transfer is a thermally activated process; besides, the lifetime increases up to 2.03 μs as expected due to the decreasing of the non-radiative transition (Figure S18).

3.5 X-ray structure determination

In order to get an explanation for the impressive photoluminescence quantum efficiency of [Pt(5-mesityl-dpyb)(SCN_4Ph)] in the solid state, its X-ray structure was investigated.

Crystals were obtained by slow evaporation from a CH_2Cl_2 solution. In this way, the platinum complex has been crystallized as dichloromethane solvate.

The coordination around the metal centre is a distorted square planar, made up of two nitrogen atoms and one carbon atom of the terdentate ligand and one sulphur atom of the thiolate ligand. As revealed by the crystal structure, there are two distinct complexes per one dichloromethane molecule within the asymmetric unit (Figure 3a). Indeed, they are stacked together to form dimeric units with the planes of the cyclometalated 1,3-di(2-pyridyl)benzene portions that are almost parallel and with a short Pt···Pt contact of 3.3659(9) Å. The Pt1-C1 bond distance is 1.921(9) Å, while Pt2-C33 = 1.923(9) Å, Pt1-N1 = 2.032(8) Å, Pt1-N2 = 2.036(8) Å, Pt1-S1 = 2.430(3) Å, Pt2-N7 = 2.024(8) Å, Pt2-N8 = 2.054(9) Å and Pt2-S2 = 2.408(3) Å. These distances are in the range of those reported for [N^C^NPt]$^+$ analogues.[33] The two complexes are

rotated with respect to each other (torsion angle C1-Pt1-Pt2-C33 = 146.6(4) Å) so that the corresponding thiolate and mesityl moieties point in opposite directions.

Besides the Pt···Pt interaction, a series of π···π interactions hold together the complexes. As regards the two cristallographycally indipendent units, the pyridine rings with N1 and N7 have an almost face-to-face alignment. Furthermore, the complex bearing the Pt1 atom interacts with two additional complexes with Pt1 and Pt2 atoms in an antiparallel slipped stacking (Figure 3b). Inter

are H···H, C···H, N···H and Cl···H interactions that drive the crystal packing (Figure 3f). For instance, a C···H interaction between C35 and H38 (i.e. C-H··· π) of the complexes bearing Pt2 atom leads to an orthogonal configuration of these complexes related by the 2_1 axis (Figure 3c). This results in zig-zag chains throughout the structure running parallel to the b axis (Figure 3d).

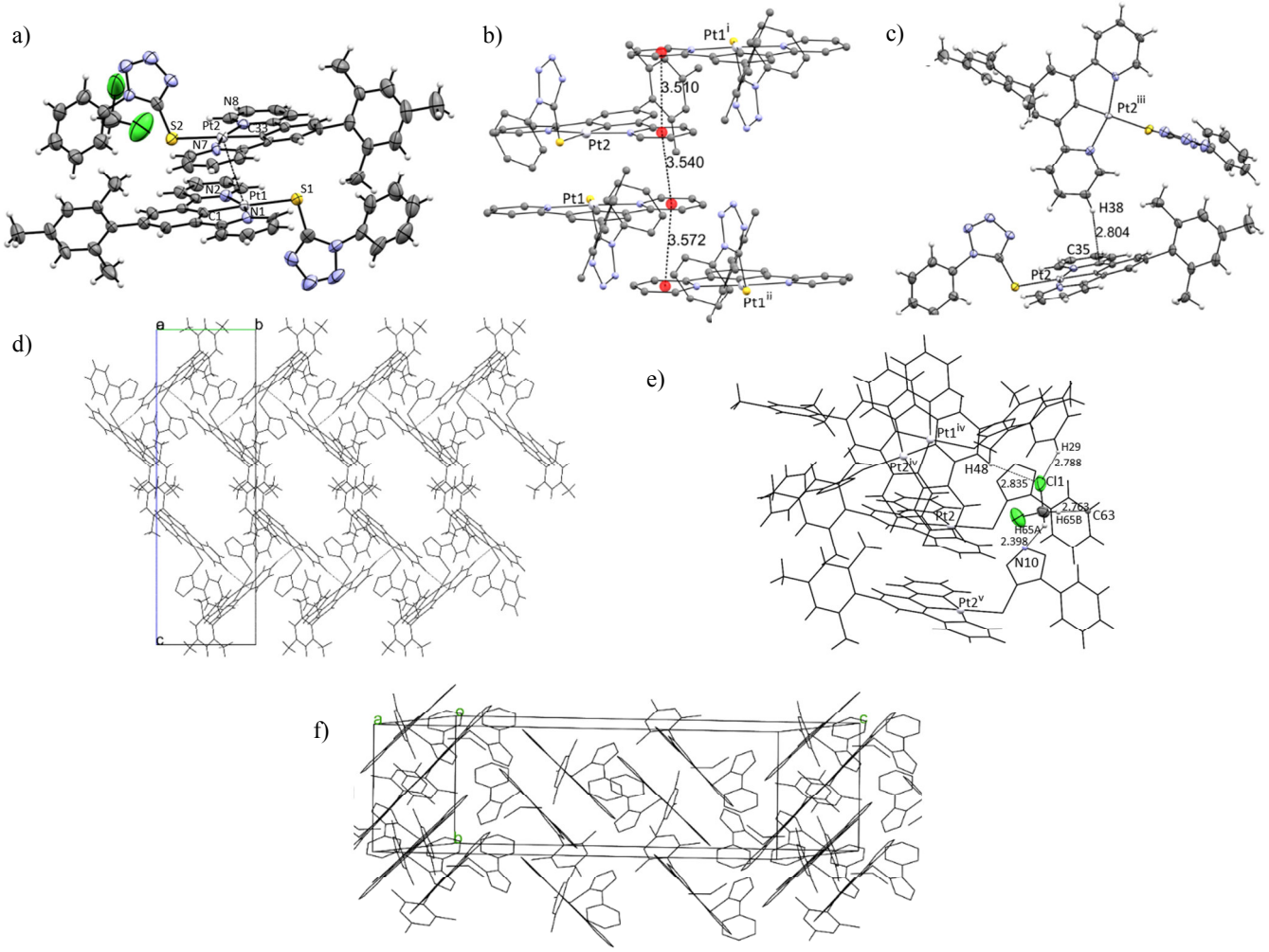

Figure 3. a) Asymmetric unit with selected atom labels and the Pt···Pt contact displayed. b) π···π stacking with selected distances between the centroids of pyridine rings (hydrogens omitted for clarity); c) C-H··· π interaction and orthogonal configuration of Pt2 bearing complexes; d) zig-zag chain of Pt2 bearing complexes; e) C···H, N···H and Cl···H interactions for dichloromethane with selected bond distances; f) crystal packing in a perspective view. Symmetry codes: i) x, 1+y, z; ii) 2-x, 2-y, -z; iii) 3/2-x, 1/2+y, 1/2-z; iv) 3/2-x, -1/2+y, 1/2-z; v) x, -1+y, z.

The particular structure of [Pt(5-mesityl-dpyb)(SCN_4Ph)] suggests that the presence of both the 1-phenyl-1H-tetrazole-5-thiolate coligand and the bulky mesityl group plays an important role in inhibiting self-quenching intermolecular π–π stacking in the solid state.

3.6 OLED and WOLED

Many platinum(II) complexes bearing a cyclometalated 1,3-di(2-pyridyl)benzene have been used as emitters in multilayer OLEDs, affording high external quantum efficiencies.[26-34] Besides, due to their inclination to give highly luminescent bimolecular aggregates or excimers, they are potentially useful for the fabrication of white OLEDs (WOLEDs), estimated to be cheaper and more efficient than fluorescent and incandescent illumination light sources.[60] In fact, a mixture of efficient triplet monomer and excimer emission is an appealing avenue to single-dopant white-emitting devices. However, until now, most OLEDs based on this kind of Pt(II) complexes have been

prepared by vacuum-sublimed techniques. Such fabrication methods, based on evaporation, are usually expensive processes. Some of us previously reported WOLEDs which use [Pt(5-methyl-dpyb)X)] (X = Cl, NCS) compounds as emitters, fabricated by spin-coating techniques, with maximum brightness of 161-195 cd m^{-2}.[31] Maximum external quantum efficiency (EQE) values (0.21-0.23 %)[31] were much lower than those reached for OLEDs fabricated by evaporation techniques with complexes of the same family,[27] but one order of magnitude higher than that of an OLED built by the spin-coating technique with a substituted 4,4'-stilbenoid N^C^N platinum (II).[61]

The relatively high solubility of the new complex [Pt(5-mesityl-dpyb)(SCN_4Ph)] prompted us to study its application for the preparation of solution-processed OLEDs. The devices were built by using both dry and wet processes (sublimation in high vacuum and spin coating) onto a pre-cleaned glass substrate made of indium tin oxide (ITO) (Experimental). Holes were injected from the ITO anode and passed through a 40 nm thick transporting layer made of PEDOT:PSS. Electrons were injected from an Al/LiF cathode and transported to the emitting layer (EML) by means of a layer of 2,2',2"-(1,3,5-benzinetriyl)-tris(1-phenyl-1-H-benzimidazole) (TPBi, 30 nm thick). Charges recombined in the 40 nm thick EML made of a 4,4',4''-tris(N-carbazolyl-triphenylamine (TCTA) matrix, hosting the [Pt(5-mesityl-dpyb)(SCN_4Ph)] (8% and 25% wt) as Pt-based emitter. EL spectra of the OLEDs are shown in Figure 4. OLED emissions are in the green and white regions; the CIE coordinates of [Pt(5-mesityl-dpyb)(SCN_4Ph)] 8% and 25% are (0.27, 0.59) and (0.40, 0.52), respectively. The EL spectra closely match the PL ones of the complex in solution at different concentration (low concentration 10^{-6} M only monomer emission and about 10^{-4} M with multi-emission from monomer and dimer species).

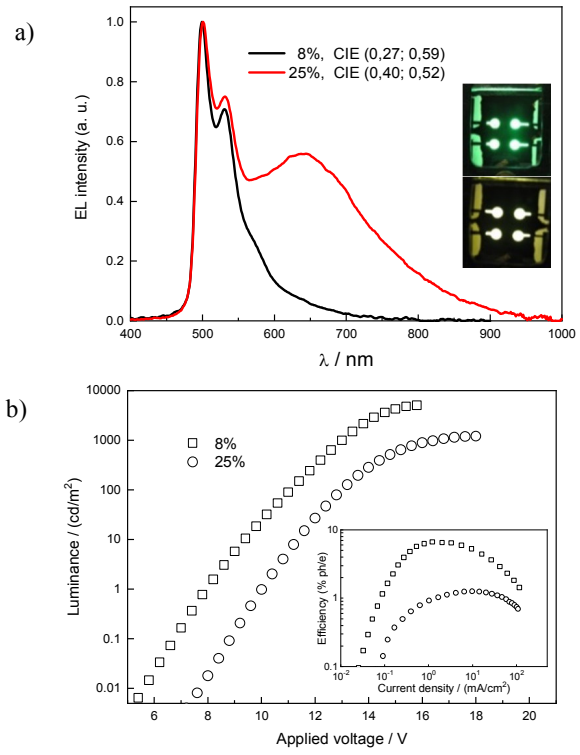

Figure 4 a) Electroluminescence spectra at 15 V of OLEDs. In the inset there are photos of green and white OLEDs based on [Pt(5-mesityl-dpyb)(SCN_4Ph)]. b) Luminance vs applied voltage and external EL efficiency vs current density (inset) of the OLEDs.

There is no significant contribution to the EL emission bands from the TBPi electron-transporting (hole-blocking) or TCTA binder layers, in agreement with a good charge carrier confinement within the EML and complete energy transfer from the excited states of TCTA (formed by charge carrier recombination) to the Pt complex.

The luminance and external EL efficiency as function of current density and applied voltage of both OLEDs are shown in Figure 4b. Luminance of ≈ 1000 cd m^{-2} at about 13 V with external EL efficiency ≈ 6% and at about 16 V with external EL efficiency ≈ 1% were obtained for green and white OLEDs, respectively. The excellent OLED performance observed with [Pt(5-mesityl-dpyb)(SCN_4Ph)] as emitter, to our knowledge, is much better with respect to those reported before for solution-processed OLEDs built with Pt complexes.[31]

4. CONCLUSION

In conclusion, a novel complex, namely [Pt(5-mesityl-1,3-di-(2-pyridyl)benzene)(1-phenyl-1H-tetrazole-5-thiolate)], was easily prepared and well characterized. Interestingly, it exhibits green and red phosphorescence in dichloromethane solution and in the solid state, respectively. In both cases the quantum yield is impressive showing for the first time that even platinum(II) complexes with a thiolate can reach excellent luminescent properties. It appears that the presence of both the 1-phenyl-1H-tetrazole-5-thiolate coligand and the mesityl bulky group play an important role in inhibiting self-quenching intermolecular π-π stacking in the solid state, thus allowing to reach large quantum yields. This new complex, characterized by an excellent solubility, is the first member of an appealing class of cyclometalated 1,3-di-(2-pyridyl)benzene platinum(II) complexes for convenient solution-processable OLEDs and WOLEDs. Our results already show that it allows to fabricate green OLEDs with maximum EQE similar to that obtained with more expensive vacuum techniques and, depending on its concentration, it is possible to tune the color of the OLED.

Conflicts of interest

There are no conflicts to declare

Acknowledgements

We deeply thank Prof. Francesco Demartin for fruitful discussions. The National Interuniversity Consortium of Materials Science and Technology (Project INSTMMI012), the Università degli Studi di Milano (Piano Sostegno alla Ricerca 2015–17-LINEA 2 Azione A – Giovani Ricercatori and PSR 2019-Linea 2 Azione A – PSR2019_DIP_005_PI_CDRAG "Coordination complexes and organic-inorganic hybrid

materials for photonics and optoelectronics"), and CNR are acknowledged for financial support.

Notes and references

1 Y. Chi and P. T. Chou, *Chem. Soc. Rev.*, 2010, **39**, 638-655.
2 M. Z. Shafikov, R. Daniels, P. Pander, F. B. Dias, J. A. G. Williams and V. N. Kozhevnikov, *ACS Appl. Mater. Interfaces*, 2019, **11**, 8182-8193.
3 L.-K. Li, M.-C. Tang, W.-L. Cheung, S.-L. Lai, M. Ng, C. K.-M. Chan, M.-Y. Chan and V. W.-W. Yam, *Chem. Mater.*, 2019, **31**, 17, 6706-6714.
4 L. F. Gildea and J. A. G. Williams in *Iridium and Platinum Complexes for OLEDs. In Organic Light-Emitting Diodes: Materials, Devices and Applications*, (Ed. A. Buckley) Woodhead: Cambridge 2013; Ch 3.
5 M. A. Baldo, D. F. O'Brien, Y. You, A. Shoustikov, S. Sibley, M. E. Thompson and S. R. Forest, *Nature*, 1998, **395**, 151-154.
6 H. Yersin, A. F. Rausch, R. Czerwieniec, T. Hofbeck and T. Fischer, *Coord. Chem. Rev.*, 2011, **255**, 2622-2652.
7 Q. Zhao, F. Li and C. Huang, *Chem. Soc. Rev.*, 2010, **39**, 3007-3030.
8 E. Baggaley, J. A. Weinstein and J. A. G. Williams, *Coord. Chem. Rev.*, 2012, **256**, 1762-1785.
9 P.-K. Chow, G. Cheng, G. S. M. Tong, W.-P. To, W.-L. Kwong, K. H. Low, C.-C. Kwok, C. Ma and C.-M. Che, *Angew. Chem. Int. Ed.*, 2015, **54**, 2084-2089.
10 K. Y. Zhang, Q. Yu, H. Wei, S. Liu, Q. Zhao and W. Huang, *Chem. Rev.*, 2018, **118**, 1770-1839.
11 J. R. Berenguer, E. Lalinde and M. T. Moreno, *Coord. Chem. Rev.*, 2018, **366**, 69-90.
12 A. Colombo, M. Fontani, C. Dragonetti, D. Roberto, J. A. G. Williams, R. Scotto di Perrotolo, F. Casagrande, S. Barozzi and S. Polo, *Chem. Eur. J.*, 2019, **25**, 7948-7952.
13 A. Aliprandi, B. N. Dimarco and L. De Cola, *Photochemistry*, 2019, **46**, 319-351.
14 J. Kalinowski, *J. Non-Cryst. Solids*, 2008, **354**, 4170-4175;
15 S. Reineke, F. Lindner, G. Schwartz, N. Seidler, K. Walzer, B. Lussem and K. Leo, *Nature*, 2009, **459**, 234-238.
16 R. Capelli, S. Toffanin, G. Generali, H. Usta, A. Facchetti and M. Muccini, *Nat. Mater.*, 2010, **9**, 496-503.
17 J. Kalinowski, V. Fattori, M. Cocchi and J.A.G. Williams, *Coord. Chem. Rev.*, 2011, **255**, 2401-2425.
18 P. Brulatti, V. Fattori, S. Muzzioli, S. Stagni, P.P. Mazzeo, D. Braga, L. Maini, S. Milita and M. Cocchi, *J. Mater. Chem. C*, 2013, **1**, 1823-1831.
19 J. A. G. Williams, A. Beeby, S. Davies, J. A. Weinstein and C. Wilson, *Inorg. Chem.*, 2003, **42**, 8609-8611.
20 S. J. Farley, D. L. Rochester, A. L. Thompson, J. A. K. Howard and J. A. G. Williams, *Inorg. Chem.*, 2005, **44**, 9690-9703.
21 J. A. G. Williams, *Chem. Soc. Rev.*, 2009, **38**, 1783-1801.
22 A. F. Rausch, L. Murphy, J. A. G. Williams and H. Yersin, *Inorg. Chem.*, 2012, **51**, 312-319.
23 A. Rodrigue-Witchel, D. L. Rochester, S.-B. Zhao, K. B. Lavelle, J. A. G. Williams, S. Wang, W. B. Connick and C. Reber, *Polyhedron*, 2016, **108**, 151-155.
24 M. M. Mdleleni, J. S. Bridgewater, R. J. Watts and P. C. Ford, *Inorg. Chem.*, 1995, **34**, 2334-2342.
25 T. C. Cheung, K. K. Cheung, S. M. Peng and C. M. Che, *J. Chem. Soc., Dalton Trans.*, 1996, 1645-1651.
26 W. Sotoyama, T. Satoh, N. Sawatari and H. Inoue, *Appl. Phys. Lett.*, 2005, **86**, 153505.
27 M. Cocchi, D. Virgili, V. Fattori, D. L. Rochester and J. A. G. Williams, *Adv. Funct. Mater.*, 2007, **17**, 285-289.
28 X. Yang, Z. Wang, S. Madakuni, J. Li and G.E. Jabbour, *Adv. Mater.*, 2008, **20**, 2405-2409.
29 M. Cocchi, J. Kalinowski, V. Fattori, J. A. G. Williams and L. Murphy, *Appl. Phys. Lett.*, 2009, **94**, 073309.
30 E. Rossi, L. Murphy, P. L. Brothwood, A. Colombo, C. Dragonetti, D. Roberto, R. Ugo, M. Cocchi and J. A. G. Williams *J. Mater. Chem.*, 2011, **21**, 15501-15510.
31 W. Mroz, C. Botta, U. Giovanella, E. Rossi, A. Colombo, C. Dragonetti, D. Roberto, R. Ugo, A.Valore and J.A.G. Williams *J. Mater. Chem.*, 2011, **21**, 8653-8661.
32 E. Rossi, A. Colombo, C. Dragonetti, D. Roberto, R. Ugo, A. Valore, L. Falciola, P. Brulatti, M. Cocchi and J.A.G. Williams, *J. Mater. Chem.*, 2012, **22**, 10650-10655.
33 E. Rossi, A. Colombo, C. Dragonetti, D. Roberto, F. Demartin, M. Cocchi, P. Brulatti, V. Fattori and J.A.G. Williams *Chem. Commun.*, 2012, **48**, 3182-3184.
34 F. Nisic, A. Colombo, C. Dragonetti, D. Roberto, A. Valore, J.M. Malicka, M. Cocchi, G.R. Freeman and J.A.G, Williams, *J. Mater. Chem. C*, 2014, **2**, 1791-1800.
35 E. Baggaley, J. A. Weinstein and J. A. G. Williams, *Coord. Chem. Rev.*, 2012, **256**, 1762-1785.
36 E. Baggaley, S. W. Botchway, J. W. Haycock, H. Morris, I. V. Sazanovich, J. A. G. Williams and J. A. Weinstein, *Chem. Sci.*, 2014, **5**, 879-886.
37 A. Colombo, F. Fiorini, D. Septiadi, C. Dragonetti, F. Nisic, A. Valore, D. Roberto, M. Mauro and L. De Cola, *Dalton Trans.*, 2015, **44**, 8478-8487.
38 Z. Wang, E. Turner, V. Mahoney, S. Madakuni, T. Groy and J. Li, *Inorg. Chem.*, 2010, **49**, 11276-11286.
39 W. A. Tarran, G. R. Freeman, L. Murphy, A. M. Benham, R. Kataky and J. A. G. Williams, *Inorg. Chem.*, 2014, **53**, 5738-5749.
40 M. J. Frisch, G. W. Trucks, H. B. Schlegel, G. E. Scuseria, M. A. Robb, J. R. Cheeseman, G. Scalmani, V. Barone, B. Mennucci, G. A. Petersson, H. Nakatsuji, M. Caricato, X. Li, H. P. Hratchian, A. F. Izmaylov, J. Bloino, G. Zheng, J. L. Sonnenberg, M. Hada, M. Ehara, K. Toyota, R. Fukuda, J. Hasegawa, M. Ishida, T. Nakajima, Y. Honda, O. Kitao, H. Nakai, T. Vreven, J. A. Montgomery, Jr., J. E. Peralta, F. Ogliaro, M. Bearpark, J. J. Heyd, E. Brothers, K. N. Kudin, V. N. Staroverov, R. Kobayashi, J. Normand, K. Raghavachari, A. Rendell, J. C. Burant, S. S. Iyengar, J. Tomasi, M. Cossi, N. Rega, J. M. Millam, M. Klene, J. E. Knox, J. B. Cross, V. Bakken, C. Adamo, J. Jaramillo, R. Gomperts, R. E. Stratmann, O. Yazyev, A. J. Austin, R. Cammi, C. Pomelli, J. W. Ochterski, R. L. Martin, K. Morokuma, V. G. Zakrzewski, G. A. Voth, P. Salvador, J. J. Dannenberg, S. Dapprich, A. D. Daniels, Ö. Farkas, J. B. Foresman, J. V. Ortiz, J. Cioslowski and D. J. Fox, *Gaussian 09, Revision D.01*, Gaussian, Inc., Wallingford CT, 2009.
41 A. D. Becke, *J. Chem. Phys.*, 1993, **98**, 5648-5652.
42 S. Grimme, S. Ehrlich and L. Goerigk, *J. Comput. Chem.*, 2011, **32**, 1456-1465.
43 A. D. McLean and G. S. Chandler, *J. Chem. Phys.*, 1980, **72**, 5639-5648.
44 A. J. H. Wachters, *J. Chem. Phys.*, 1970, **52**, 1033.
45 A. Petersson and M. A. Al-Laham, *J. Chem. Phys.*, 1991, **94**, 6081.
46 P. J. Hay and W. R. Wadt, *J. Chem. Phys.*, 1985, **82**, 299.
47 S. Miertus, E. Scrocco and J. Tomasi, *Chem. Phys.*, 1981, **55**, 117-129.
48 M. Cossi, V. Barone, R. Cammi and J. Tomasi, *Chem. Phys. Lett.*, 1996, **255**, 327-335.
49 V. Barone and M. Cossi, *J. Phys. Chem. A*, 1998, **102**, 1995-2001.
50 M. Cossi, N. Rega, G. Scalmani and V. Barone, *J. Comput. Chem.*, 2003, **24**, 669-681.
51 SADABS Area-Detector Absorption Correction Program; Bruker AXS: Madison, WI, 2000.

52 A. Altomare, M.C. Burla, M. Camalli, G.L. Cascarano, C. Giacovazzo, A. Guagliardi, A.G.G. Moliterni, G. Polidori and R. Spagna, *J. Appl. Crystallogr.*, 1999, ***32***, 115-119.
53 G.M. Sheldrick, *Acta Crystallogr., Sect. A*, 2008, **64**, 112-122.
54 L.J. Farrugia, *J. Appl. Crystallogr.*, 1999, **32**, 837.
55 H. Imoto, S. Tanaka, T. Kato, S, Watase, K. Matsukawa, T. Yumura and K. Naka, *Organometallics*, 2016, **35**, 364-369.
56 P. H. Lanoë, A. Moreno-Betancourt, L. Wilson, C. Philouze, C. Monnereau, H. Jamet, D. Jouvenot and F. Loiseau, *Dyes and Pigments*, 2019, **162**, 967-977.
57 X. Wang, Y. L. Chang, J. S. Lu, T. Zhang, Z. H. Lu and S. Wang, *Adv. Funct. Mater.*, 2014, **24**, 1911-1927.
58 G. R. Kumar and P. Thilagar, *Inorg. Chem.*, 2016, **55**, 12220-12229.
59 L. Ricciardi, M. La Deda, A. Ionescu, N. Godbert, I. Aiello and M. Ghedini, *Dalton Trans*., 2017, **46**, 12625-12635.
60 B. W. D'Andrade, *Nat. Photonics*, 2007, **1**, 33-34.
61 G.D. Batema, M. Lutz, A. L. Spek, C. A. van Walree, C. de Mello Donegà, A. Meijerink, R. W. A. Havenith, J. Pérez-Moreno, K. Clays, M. Buchel, A.van Dijken, D. L. Bryce, G. P. M. van Klink and G. van Koten, *Organometallics*, 2008, **27**, 1690-1701.